

Propagation of obliquely incident water waves over a trench. Part 2. Currents flowing along the trench

By JAMES T. KIRBY

Coastal and Oceanographic Engineering Department, University of Florida,
Gainesville, FL 32611, USA

ROBERT A. DALRYMPLE AND SEUNG NAM SEO

Department of Civil Engineering, University of Delaware, Newark, DE 19716, USA

(Received 17 December 1985 and in revised form 23 July 1986)

Several methods based on matched eigenfunction expansions are developed to study the diffraction of a linear, steady train of waves in finite water depth by a combination of straight depth discontinuities and colinear vortex sheets, where the vortex sheets represent a first approximation to a thin shear layer between regions of dissimilar ambient current velocity. Special attention is paid to the case of a current flowing along a submerged trench, and predictions of reflection and transmission are seen to be highly sensitive to the magnitude and direction of the ambient current.

1. Introduction

The assumption that vertical shear layers of small thickness may be approximated at leading order by vertical vortex sheets leads to a major simplification in the study of water waves diffracted by strong shear in an ambient current. Using this assumption, the wave motion in each region of constant current speed (with the regions joined at vortex sheets) may be assumed to be irrotational, and therefore the diffraction problem may be formulated using potential theory. Evans (1975) formulated the appropriate boundary-value problem for a single vortex sheet in water of arbitrary depth, and obtained solutions for deep water using a Galerkin approximation to the resulting integral equation. Smith (1983) has extended Evans' work to the case of a current jet bounded by two vortex sheets, and developed a reasonably successful plane-wave approximation using only progressive wave modes and a depth-averaging procedure at the vortex sheet which incorporates the mismatch between the fluid velocities induced by the propagating wave modes. Smith (1987) has further extended his depth-averaging procedure to cover the case of a concurrent shelf and vortex sheet, and has also extended Miles' (1967) variational scattering approximation for a shelf to include the presence of a vortex sheet.

The same problem posed in shallow-water theory has also drawn some attention. Mollo-Christensen (1978) considered the possibility of resonant over-reflection at a vortex sheet, using a formulation given by Miles (1957) for the corresponding acoustical problem. Mei & Lo (1984, see corrections, 1986) considered the current-jet problem. Kirby (1986) has shown that the appropriate matching conditions between regions in shallow-water theory are derivable by a depth average of Evans' (1975) conditions, and essentially guarantee that volume flux normal to the displaced vortex

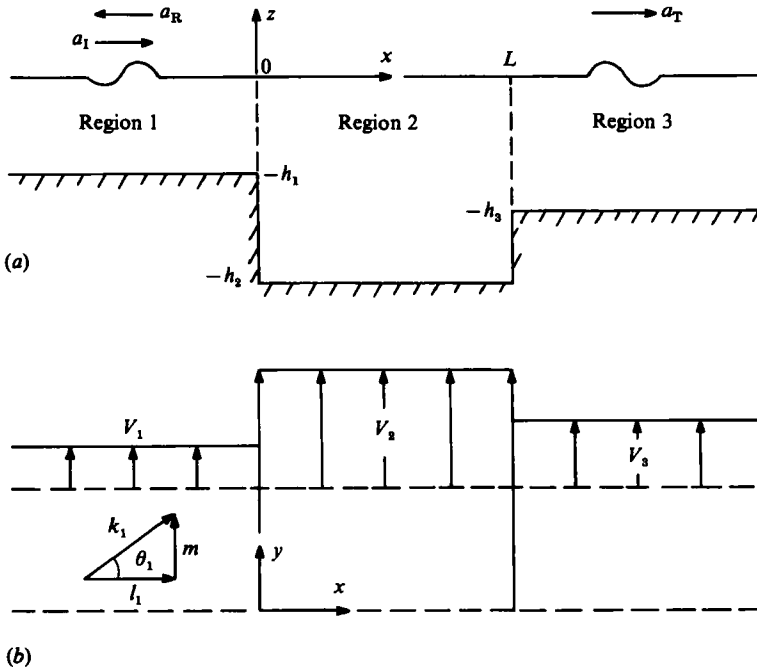


FIGURE 1. Physical domain for the case of an asymmetric trench of width L . Incident waves in region 1. (a) elevation; (b) plan.

sheet is conserved. Kirby then formulated the shallow-water problem for coincident vortex sheet and sudden depth change; the formulation is analogous to Lamb's (1945) treatment of a step and is likely to be the correct matching condition to the same level of accuracy as Lamb's.

Vortex sheets disturbed by wave motions are likely to be unstable (Miles 1958), and thus it is not known how much physical relevance to attach to the results surveyed above. For this reason, and because of its engineering relevance, we choose here to study the case of a uniform current flowing along a trench, bounded by shallower regions which may be expected to have currents of lower or zero velocity. This case may serve as a first approximation to tidal flow along a natural or dredged channel. Further, the presence of rigid surfaces bounding a portion of the isolated large current may serve to guide the current and stabilize the position of the current boundaries in a practical sense.

The theory of wave diffraction at depth discontinuities in a stationary domain is well developed; a review of results that are relevant here may be found in Kirby & Dalrymple (1983, hereinafter referred to as KD1) and in Smith (1987). The purpose of this study is to extend the results of KD1 to include the effects of currents flowing parallel to the trench boundary. A schematic of the general problem is shown in figure 1. The problem is formulated for intermediate water depth in terms of the discrete eigenfunction expansion for each region of uniform depth and current. We then solve the full linear problem, truncated to a finite number of non-propagating wave modes, using Takano's (1960) method as in KD1. This method, denoted by EFEM below, has been verified in comparison with several computational techniques and in comparison with laboratory data by KD1. Results of a boundary-integral (BIEM) method are included for verification, and numerical results are discussed in §4. In

§5 we formulate several approximate solutions. A plane-wave solution for propagating modes is developed using the depth-averaging scheme for the full problem. Deep-water limits are compared with Smith's (1983) results and are shown to not behave as well in strong adverse currents, when each solution is compared with Evans' (1975) integral-equation solution. The plane-wave scheme is then modified in the intermediate-depth formulation to conform to the depth-averaging approach applied by Smith (1983, 1987) in his action-based model. Finally, a variational approximation following Miles (1967) is constructed and is seen to perform better than the other approximations. In §6 results in the shallow-water limit are shown to be equivalent to the results of Kirby (1986), and we investigate the effect of varying wave conditions and geometry on the reflection process.

2. The Boundary-value problem

We consider the diffraction of monochromatic, small-amplitude waves by abrupt changes in depth and ambient current. The domain is allowed to vary in the x -direction and is uniform in the y -direction, with the ambient current oriented in the y -direction. We further assume that depth variations are limited to step discontinuities, and that current variations are limited to discrete vortex sheets coinciding with the depth variations, as shown in figure 1. These restrictions allow the fluid domain to be considered as a set of regions, each with constant parameters. The flow in each region is considered to be inviscid and irrotational, and each region's velocity potential ϕ_i ($i = 1, 2, 3$) may then be expressed in terms of a complete set of eigenfunctions.

The problem in each region is then given by

$$\nabla^2 \phi_i = \frac{\partial^2 \phi_i}{\partial x^2} + \frac{\partial^2 \phi_i}{\partial y^2} + \frac{\partial^2 \phi_i}{\partial z^2} = 0, \quad -h_i \leq z \leq 0, \quad (2.1)$$

$$\frac{\partial \tilde{\eta}_i}{\partial t} + V_i \frac{\partial \tilde{\eta}_i}{\partial y} = \frac{\partial \phi_i}{\partial z}, \quad z = 0, \quad (2.2)$$

$$g \tilde{\eta}_i + \frac{\partial \phi_i}{\partial t} + V_i \frac{\partial \phi_i}{\partial y} = 0, \quad z = 0, \quad (2.3)$$

$$\frac{\partial \phi_i}{\partial z} = 0, \quad z = -h_i. \quad (2.4)$$

We assume that the wave motion in all regions is driven by a wave that is incident from $x = -\infty$ in region 1, propagating at angle θ_1 to the x -direction. We then have

$$m = k_1 \sin \theta_1 = \text{constant for all } i \quad (2.5)$$

owing to the requirement of conservation of wave crests in the y -direction, where k_1 is the real wavenumber in region 1 as defined below.

At the discontinuities $x = x_{ij}$ between regions i and j , the appropriate boundary conditions may be obtained from Evans (1975). Omitting the details, which may be found in that paper, we impose continuity of normal flow following the vortex sheet $\zeta_{ij}(y, z, t)$ at x_{ij} ,

$$\frac{\partial \phi_i}{\partial x} = \frac{\partial \zeta_{ij}}{\partial t} + V_i \frac{\partial \zeta_{ij}}{\partial y}, \quad (2.6a)$$

$$\frac{\partial \phi_j}{\partial x} = \frac{\partial \zeta_{ij}}{\partial t} + V_j \frac{\partial \zeta_{ij}}{\partial y}; \quad -(h_i, h_j)_{\min} \leq z \leq 0, \quad (2.6b)$$

and continuity of pressure at x_{ij}

$$\frac{\partial \tilde{\phi}_i}{\partial t} + V_i \frac{\partial \tilde{\phi}_i}{\partial y} = \frac{\partial \tilde{\phi}_j}{\partial t} + V_j \frac{\partial \tilde{\phi}_j}{\partial y}; \quad -(h_i, h_j)_{\min} \leq z \leq 0. \quad (2.7)$$

Finally, we set $\partial \phi_i / \partial x = 0$ on any submerged vertical boundary.

Imposing the conditions of the incident wave on the problem, we may write

$$\tilde{\phi}_i(x, y, z, t) = \phi_i(x, z) e^{i(my - \omega t)}, \quad (2.8)$$

$$\tilde{\eta}_i(x, y, t) = \eta_i(x) e^{i(my - \omega t)}, \quad (2.9)$$

where ω is the absolute wave frequency in stationary coordinates. The boundary-value problem for ϕ_i in each region becomes

$$\frac{\partial^2 \phi_i}{\partial x^2} + \frac{\partial^2 \phi_i}{\partial z^2} - m^2 \phi_i = 0, \quad -h_i \leq z \leq 0, \quad (2.10)$$

$$g \frac{\partial \phi_i}{\partial z} + \sigma_i^2 \phi_i = 0, \quad z = 0, \quad (2.11)$$

$$\frac{\partial \phi_i}{\partial z} = 0, \quad z = -h_i, \quad (2.12)$$

$\sigma_i = \omega - mV_i$ is the wave frequency relative to the ambient current. The boundary conditions reduce to

$$\frac{1}{\sigma_i} \frac{\partial \phi_i}{\partial x} = \frac{1}{\sigma_j} \frac{\partial \phi_j}{\partial x}, \quad x = x_{ij}, \quad -(h_i, h_j)_{\min} \leq z \leq 0 \quad (2.13)$$

$$\text{and} \quad \sigma_i \phi_i = \sigma_j \phi_j; \quad x = x_{ij}, \quad -(h_i, h_j)_{\min} \leq z \leq 0. \quad (2.14)$$

Equations (2.10)–(2.12) have the solution

$$\phi_i = \sum_{n=0}^{\infty} f_{i,n}(z) \hat{\phi}_{i,n}(x), \quad (2.15)$$

where

$$f_{i,0}(z) = \cosh k_i(h_i + z), \quad (2.16)$$

$$f_{i,n}(z) = \cos(K_{i,n}(h_i + z)); \quad n = 1, \dots, \infty, \quad (2.17)$$

and where k_i is the one real root of

$$\sigma_i^2 = gk_i \tanh k_i h_i \quad (2.18a)$$

and $K_{i,n}$ are the infinity of real roots of

$$\sigma_i^2 = -gK_{i,n} \tan K_{i,n} h_i, \quad (2.18b)$$

which are ordered from smallest to largest. The set of functions $\{f_{i,n}, n = 0, 1, \dots\}$ form a complete orthogonal basis for region i . The forms of solutions $\hat{\phi}_{i,n}$ can vary significantly depending on the values of σ_i and k_i .

Case 1: $\sigma_i > 0, k_i > m$

$$\text{Then} \quad \phi_i = \{A_i^\pm e^{\pm i k_i x}\} f_{i,0}(z) + \sum_{n=1}^{\infty} \{B_{i,n}^\pm e^{\pm \lambda_{i,n} x}\} f_{i,n}(z), \quad (2.19)$$

where
$$l_i = (k_i^2 - m^2)^{\frac{1}{2}}, \quad \lambda_{i,n} = (K_{i,n}^2 + m^2)^{\frac{1}{2}} \quad (2.20)$$

and where the \pm indicates the sum over left- and right-propagating (or decaying) components. The complete solution consists of two freely propagating waves and a double infinity of evanescent modes.

Case 2: $\sigma_i > 0, k_i = m$

In this case the freely propagating portion of (2.19) is reduced to

$$\phi_i = \{A_i + A'_i x\} f_{i,0}(z) \quad (2.21)$$

with the evanescent modes unaltered.

Case 3: $\sigma_i > 0, k_i < m$

Then
$$\phi_i = \{A_i^\pm e^{\pm \lambda_{i,0} x}\} f_{i,0}(z) + \sum_{n=1}^{\infty} \{B_{i,n}^\pm e^{\pm \lambda_{i,n} x}\} f_{i,n}(z), \quad (2.22)$$

with
$$\lambda_{i,0} = (m^2 - k_i^2)^{\frac{1}{2}} > 0. \quad (2.23)$$

Case 4: $\sigma_i = 0$

This represents a special case where the wave phase speed in the y -direction coincides with the ambient-current speed V_i in region i . Then $k_i = K_{i,n} = 0$ in (2.18). From (2.10)–(2.12) we find that

$$\phi_i = A_i^\pm e^{\pm mx}, \quad (2.24)$$

while (2.13) requires
$$\frac{\partial \phi_i}{\partial x} = 0; \quad x = x_{ij}, \quad (2.25)$$

which gives $A_i^+ = A_i^-$. In a semi-infinite region i , we then obtain $A_i^+ = A_i^- = 0$ owing to boundedness conditions; no wave-induced motion of any sort can occur in region i . In a finite region i , (2.3) implies $\eta_i = 0$. For $0 \leq x_i \leq L$ and (2.25) applied at 0 and L , we get

$$m(A_i^+ - A_i^-) = m(A_i^+ e^{mL} - A_i^- e^{-mL}) = 0, \quad (2.26)$$

which again requires $A_i^+ = A_i^- = 0$. Thus, any region of non-vanishing width in which $\sigma_i = 0$ represents a totally impenetrable barrier to wave motion incident on it.

Case 5: $\sigma_i < 0$

The possible cases for $\sigma_i < 0$ mimic the set of three cases with $\sigma_i > 0$, with the exception that the negative branch of roots for the l_i and $\lambda_{i,0}$ must be taken. For $\sigma_i < 0$ and $|k_i| > m$, the situation corresponding to over-reflection can occur. This theoretically predicted phenomenon has been discussed by Mollo-Christensen (1978) in the context of shallow-water waves. A schematic of the dispersion relation and possible resulting flow conditions in region i is given in figure 2. The plot clearly shows the tendency for following currents, $V_i > 0$, to drive the relative frequency σ_i down to or beyond the zero value, rendering the region i more reflective, while adverse or opposing currents $V_i < 0$ may render highly reflective regions (Case 3) much less reflective by shifting them over to Case 1 behaviour.

We restrict our attention in the following discussion to Case 1 solutions in region

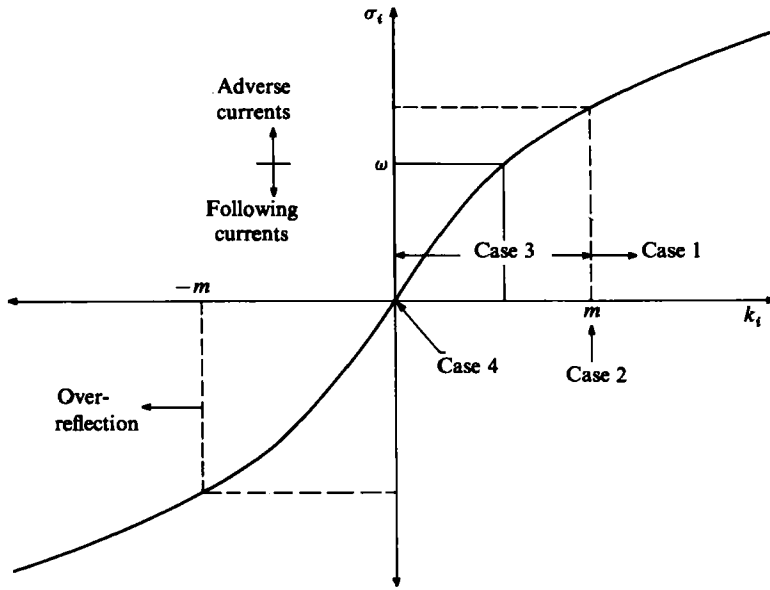


FIGURE 2. Possible solution types in region i , depending on magnitude and direction of current and value of absolute frequency ω .

1 and consider an incident wave of unit amplitude $A_1^+ = 1$. The amplitude of surface displacements for the incident and reflected wave are then

$$\left. \begin{aligned} a_I &= g^{-1}\sigma_1 \cosh k_1 h_1, \\ a_R &= g^{-1}\sigma_1 |A_1^-| \cosh k_1 h_1. \end{aligned} \right\} \quad (2.27)$$

For $k_3 \geq m$, transmitted waves may exist in region 3 with surface amplitude

$$a_T = g^{-1}\sigma_3 |A_3^+| \cosh k_3 h_3. \quad (2.28)$$

We define a reflection coefficient K_R and a transmission coefficient K_T according to

$$K_R = \frac{a_R}{a_I} = |A_1^-|, \quad K_T = \frac{a_T}{a_I} = |A_3^+| \frac{\sigma_3 \cosh k_3 h_3}{\sigma_1 \cosh k_1 h_1}. \quad (2.29)$$

Conservation of action in the diffracted-wave field then requires

$$K_R^2 + K_T^2 \left\{ \frac{n_3 k_1^2 l_3}{n_1 k_3^2 l_1} \right\} = 1$$

or

$$K_R^2 + K_T^2 \left\{ \frac{n_3 \sin 2\theta_3}{n_1 \sin 2\theta_1} \right\} = 1, \quad (2.30)$$

as given by KD1 and Evans (1975) for deep water. Here

$$n_i = \frac{\partial \sigma_i / \partial k_i}{\sigma_i / k_i} = \frac{1}{2} \left(1 + \frac{2k_i h_i}{\sinh 2k_i h_i} \right).$$

3. Numerical formulations

As in KD1, the problem formulated in §2 is first solved following the method devised by Takano (1960), which proceeds by constructing an infinite set of algebraic equations for the unknown amplitude components. We then consider the extension of the boundary-integral-equation method (BIEM) to the case of discrete regions in which irrotational flow may be assumed, and in which an ambient steady current exists.

3.1. Solution by matched eigenfunction expansions (EFEM)

Following KD1, we first truncate the series expansions for the ϕ_i to N terms. We consider the case of three regions $i = 1, 2, 3$ as in figure 1, where we denote $x_{12} = 0$ and $x_{23} = L$. In principle, a different number N may be chosen for each region; here, N is chosen to be equivalent in all three regions considered. Assuming an incident wave of unit amplitude in region 1 and applying the appropriate radiation and boundedness conditions leaves a set of $(4N+4)$ unknowns $A_1^-, B_{1,n}^+, A_2^\pm, B_{2,n}^\pm, A_3^+, B_{3,n}^-$, $n = 1, \dots, N$ as in KD1. We then employ the matching conditions on $\partial\phi_i/\partial x$ and orthogonality to obtain

$$\left. \begin{aligned} \frac{1}{\sigma_1} \int_{-h_1}^0 \frac{\partial\phi_1}{\partial x}(0, z) f_{2,n}(z) dz &= \frac{1}{\sigma_2} \int_{-h_1}^0 \frac{\partial\phi_2}{\partial x}(0, z) f_{2,n}(z) dz \\ &= \frac{1}{\sigma_2} \int_{-h_2}^0 \frac{\partial\phi_2}{\partial x}(0, z) f_{2,n}(z) dz \end{aligned} \right\} (n = 0, \dots, N), \quad (3.1a)$$

$$\left. \begin{aligned} \frac{1}{\sigma_3} \int_{-h_3}^0 \frac{\partial\phi_3}{\partial x}(L, z) f_{2,n}(z) dz &= \frac{1}{\sigma_2} \int_{-h_3}^0 \frac{\partial\phi_2}{\partial x}(L, z) f_{2,n}(z) dz \\ &= \frac{1}{\sigma_2} \int_{-h_2}^0 \frac{\partial\phi_2}{\partial x}(L, z) f_{2,n}(z) dz \end{aligned} \right\} (n = 0, \dots, N), \quad (3.1b)$$

where we have assumed $h_2 \geq (h_1, h_3)_{\max}$ for simplicity. We then employ the condition on continuity of pressure to obtain

$$\sigma_1 \int_{-h_1}^0 \phi_1(0, z) f_{1,n}(z) dz = \sigma_2 \int_{-h_1}^0 \phi_2(0, z) f_{1,n}(z) dz \quad (n = 0, \dots, N), \quad (3.2a)$$

$$\sigma_3 \int_{-h_3}^0 \phi_3(L, z) f_{3,n}(z) dz = \sigma_2 \int_{-h_3}^0 \phi_2(L, z) f_{3,n}(z) dz \quad (n = 0, \dots, N), \quad (3.2b)$$

Equations (3.1) and (3.2) give $(4N+4)$ algebraic equations for the unknown amplitudes, which may be solved as a linear matrix equation after evaluating the required integrals.

3.2. Solution by the boundary-integral-equation method (BIEM)

In order to verify the eigenfunction expansion method (EFEM), we utilize a hybrid boundary-integral-equation method. Following Yeung (1975), we distribute nodal points and boundary elements along the boundary of region 2, as shown in figure 3. We assume the value $\phi_2(x_i, z_i)$ at any nodal point (x_i, z_i) to be constant over the surrounding element. Letting (x_i, z_i) denote a nodal point located on the boundary Γ of region 2, we may express the solution $\phi_2(x_i, z_i)$ in terms of the integral over the entire boundary as

$$\phi_2(x_i, z_i) = \pi^{-1} \int_{\Gamma} \left\{ \phi_2(\xi, \eta) \frac{\partial}{\partial n} G(\xi, \eta; x_i, z_i) - G(\xi, \eta; x_i, z_i) \frac{\partial}{\partial n} \phi_2(x_i, z_i) \right\} ds, \quad (3.3)$$

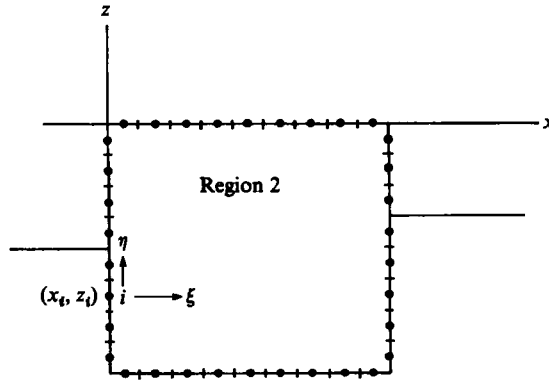


FIGURE 3. Coordinate system and boundary discretization for BIEM method.

where in the numerical method the integral becomes a sum over the finite number of boundary elements. In (3.3), $\partial/\partial n$ denotes outward normal derivative and $\{\xi, \eta\}$ are local coordinates defined in figure 3. The Green function in (3.3) is derived from the modified Helmholtz equation (2.10) and is given by

$$G(\xi, \eta; x_i, z_i) = -K_0(mr), \quad r = (\xi^2 + \eta^2)^{\frac{1}{2}}, \quad (3.4)$$

where K_0 is the modified Bessel function of the second kind and of order zero.

Following Yeung (1975) and Liu & Abbaspour (1982), we match the bounded domain 2 to the external semi-infinite regions 1 and 3 using the matching conditions (2.13). The number of terms in the expansions (2.15) for the exterior regions is then equivalent to the number of nodal points distributed over the vertical junction with that region. The resulting integrals may be evaluated using the special Gaussian quadrature integral (25.4.44) in Abramowitz & Stegun (1965). Applying the conditions (2.11) and (2.12) on the mean water surface and solid bottom and evaluating the remaining integrals leads to a linear matrix equation with solution vector containing the unknown $A_1^-, B_{1,n}^+, A_3^+, B_{3,n}^-$ ($n = 1, \dots, N$) and values of ϕ_2 at nodal points on the surface, bottom and vertical trench walls.

4. Numerical results

Since the present formulation is tailored to the intermediate-depth case with discrete evanescent mode spectrum, comparison with the previously published deep-water results of Evans (1975) or Smith (1983) is difficult. We attempt such a comparison in figure 4 for the case of a single vortex sheet, with the conditions $h_1 = h_2 = h_3$, $V_1 = 0$ and $V_2 = V_3$. We take $k_1 h_1 = 10$ in order to mimic the deep-water case and set $N = 10$. We found that the resulting coefficient matrix becomes ill-conditioned for some large negative values of V_2/C_0 ; figure 4 presents the comparison with Evans' results over the range where solutions were obtained, for angles of incidence $\theta_1 = 15^\circ, 30^\circ, 60^\circ$ and 75° . Here, C_0 denotes the deep-water wave speed $(g/k)^{\frac{1}{2}}$.

In order to test the correspondence between the EFEM and the BIEM results, we next consider the case of a single vortex sheet over a flat bottom in intermediate depth. Figure 5 shows predicted transmission coefficient K_T as a function of Froude number $F = V_2(g h_2)^{-\frac{1}{2}}$ characterizing the current. Results for values of $k_1 h_1 = 0.1$ and 1.0 are shown, for angles of incidence $15^\circ, 30^\circ, 60^\circ$ and 75° , and with $N = 10$. The

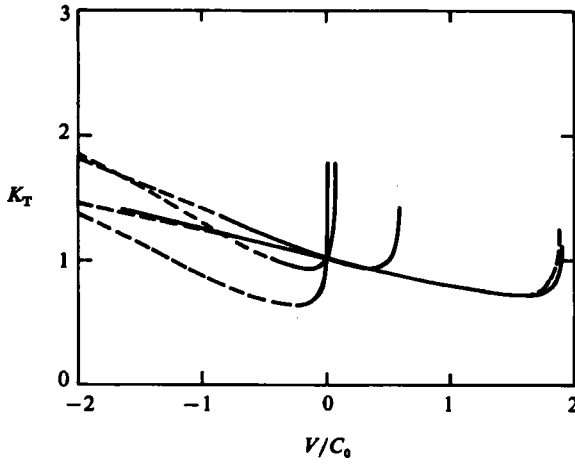


FIGURE 4. Comparison of finite-depth ($k_1 h_1 = 10$) results with Evans (1975) deep-water results for a single vortex sheet: ---, Evans; —, present results (EFEM).

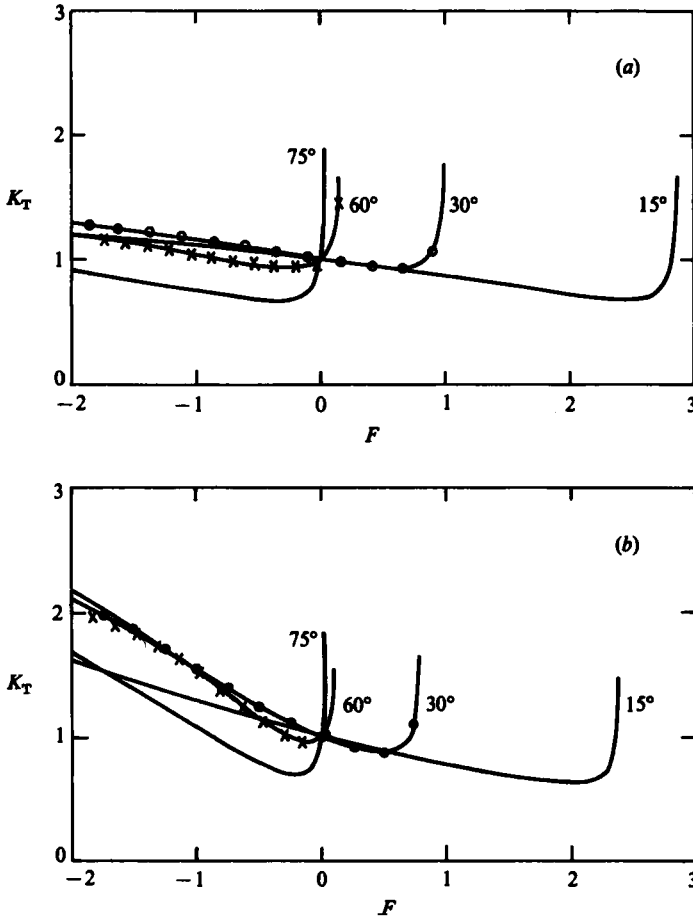


FIGURE 5. Comparison of EFEM and BIEM results in finite water depth; single vortex sheet over a flat bottom: —, EFEM results; individual marks indicate BIEM calculations. (a) $k_1 h_1 = 0.1$; (b) 1.0.

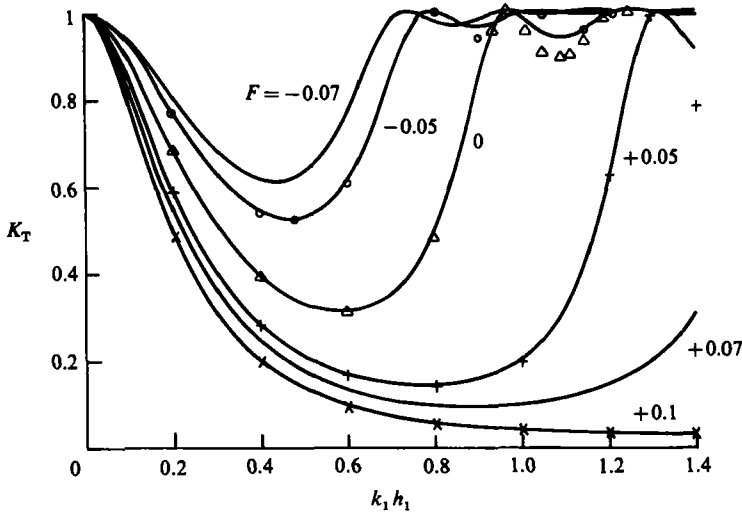


FIGURE 6. Wave transmission over a symmetric trench. $h_3 = h_1$, $V_3 = V_1 = 0$; $h_2 = 3h_1$, $L = 10h_1$, $\theta = 45^\circ$, $F = V_2/(gh_2)^{1/2}$. —, EFEM method; individual points denote BIEM calculations.

<i>N</i>	<i>F</i> = 0		<i>F</i> = -0.0525		<i>F</i> = 0.0525	
	<i>K_R</i>	<i>K_R</i>	<i>K_R</i>	<i>K_T</i>	<i>K_R</i>	<i>K_T</i>
2	0.93970	0.34200	0.58616	0.82292	0.98951	0.14446
4	0.94080	0.33895	0.57593	0.81750	0.98964	0.14356
8	0.94109	0.33816	0.57673	0.81694	0.98968	0.14331
16	0.94130	0.33757	0.57794	0.81608	0.98970	0.14314
32	0.94137	0.33738	0.57830	0.81582	0.98971	0.14309
50	0.94139	0.33732	0.57844	0.81572	0.98971	0.14307

TABLE 1. Convergence of EFEM results with increasing *N*: $h_2/h_1 = 3$, $L/h_1 = 10$, $k_1 h_1 = 0.68034$

BIEM is also applied to this case, with region 2 taken with the left boundary at the vortex sheet and the right boundary placed several water depths away. Results of the BIEM for $\theta_1 = 30^\circ$ and 60° are included and agree well with the EFEM results.

As a further check of accuracy, we found that wave action was conserved in the scattered-wave field up to the limit of precision in the calculations for all results employing the EFEM. The BIEM results exhibit some degradation of accuracy in this sense (up to $\approx 1\%$ loss in some cases), with error being reduced with increasing number of nodal points, indicating relatively slow convergence of BIEM solutions with increasing resolution of the boundary curve.

We turn now to the case of interest and give results in figure 6 for a symmetric trench with $h_2 = 3h_1$, $L = 10h_1$ and $\theta_1 = 45^\circ$. Results are given for a range of Froude numbers $-0.07 \leq F \leq 0.1$, where *F* characterizes the current in the trench. The effect of even small following or adverse currents on the transmission process is clearly apparent. As expected, adverse currents render the trench less reflective and following currents increase reflection, owing to the shift of behaviour of the motion in region 2 over the range of Cases 1–3, as described in §2.

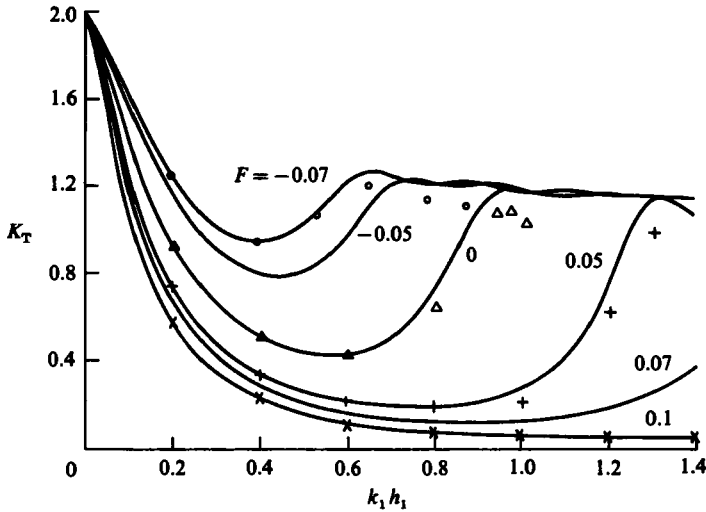


FIGURE 7. Wave transmission over an asymmetric trench. $h_3 = 2h_1$, $V_3 = V_1 = 0$; $h_2 = 3h_1$, $L = 10h_1$, $\theta_1 = 45^\circ$. Symbols as in figure 6.

Table 1 gives results of convergence tests for the EFEM method for the symmetric-trench case. For the fairly small depth change involved here, convergence is seen to be rapid except for the opposing-current example. The results for the plots in figures 6 and 7 were obtained using $N = 10$, which is sufficiently accurate for graphical purposes.

Figure 6 also shows BIEM results, indicated by isolated points. We found that BIEM results were essentially in agreement with EFEM results for configurations corresponding to Case 3 behaviour in region 2 (ϕ_2 varying exponentially across the trench). For $k_1 h_1$ greater than the value giving the first point of complete transmission $K_T = 1$, BIEM results start to differ from EFEM results. The results in figure 6 are based on retaining five non-propagated modes in the BIEM calculations. Experiments indicate that increasing the number of boundary elements on the surface and solid boundaries (for a fixed number of wave modes) decreases the difference between BIEM and EFEM results, indicating that the error is due to resolution of the variation in ϕ_2 in BIEM; however, convergence to the EFEM result is very slow with increasing number of boundary elements, and accurate results were not obtained for these regions in the present study. As a result, the BIEM results here serve mainly as a check that the EFEM model is correctly formulated.

Figure 7 presents results for an asymmetric geometry, with $h_2 = 3h_1$, $h_3 = 2h_1$, $L = 10h_1$ and $\theta_1 = 45^\circ$, and with $V_1 = V_3 = 0$. The strong dependence of K_T on small variations in current speed V_2 along the trench is again apparent. As in the previous example, BIEM results are seen to exhibit slow numerical convergence in the range of Case 1 behaviour in region 2, and in all cases the EFEM results are to be regarded as the accurate solution.

5. Approximate solution techniques

If depth changes between the trench region and external regions are not severe, KDI showed that the reflection and transmission coefficients were reasonably well predicted (for the case of no currents) by a plane-wave approximation which neglects

the influence of the evanescent modes. We shall now investigate the utility and limitations of the plane-wave approximation in the present case. We then go on to consider solutions based on an 'action-based' model following Smith (1983, 1987) and a variational formulation following Miles (1967).

5.1. Plane-wave approximation

Neglecting evanescent modes in (3.1) and (3.2) reduces the set of equations to

$$\frac{l_1}{\sigma_1} (1 - A_1^-) I_{12} = \frac{l_2}{\sigma_2} (A_2^+ - A_2^-) I_{22}, \quad (5.1a)$$

$$\frac{l_3}{\sigma_3} A_3^+ I_{32} e^{il_3 L} = \frac{l_2}{\sigma_2} (A_2^+ e^{il_2 L} - A_2^- e^{-il_2 L}) I_{22} \quad (5.1b)$$

and
$$\sigma_1 (1 + A_1^-) I_{11} = \sigma_2 (A_2^+ + A_2^-) I_{12}, \quad (5.2a)$$

$$\sigma_3 A_3^+ I_{33} e^{il_3 L} = \sigma_2 (A_2^+ e^{il_2 L} + A_2^- e^{-il_2 L}) I_{32}, \quad (5.2b)$$

where
$$I_{ij} = \int_{-(h_i, h_j)_{\min}}^0 f_{i,0}(z) f_{j,0}(z) dz. \quad (5.3)$$

Equations (5.1) and (5.2) are solved to obtain

$$A_3^+ = \frac{2\alpha\beta(I_{32}/I_{12}) e^{-il_3 L}}{(\alpha\beta' + \alpha'\beta) \cos l_2 L - i(\alpha\alpha' + \beta\beta') \sin l_2 L}, \quad (5.4a)$$

$$A_1^- = \frac{(\alpha'\beta - \alpha\beta') \cos l_2 L + i(\alpha\alpha' - \beta\beta') \sin l_2 L}{-(\alpha\beta' + \alpha'\beta) \cos l_2 L + i(\alpha\alpha' + \beta\beta') \sin l_2 L}, \quad (5.4b)$$

where

$$\alpha = l_1 I_{12}^2 \frac{\sigma_2}{\sigma_1}, \quad \alpha' = l_3 I_{32}^2 \frac{\sigma_2}{\sigma_3}, \quad \beta = l_2 I_{11} I_{22} \frac{\sigma_1}{\sigma_2}, \quad \beta' = l_2 I_{33} I_{22} \frac{\sigma_3}{\sigma_2}, \quad (5.5)$$

Equation (5.4) is equivalent to the result in KD1 (their equation (4.2)) with the exception of the appearance of the relative frequencies in the α and β values in (5.5). For the symmetric case ($V_1 = V_3$, $h_1 = h_3$) we have

$$\alpha = \alpha', \quad \beta = \beta'.$$

The solution may be recast into the form appearing in Mei & Lo (1984) and Kirby (1986) by the choice of notation

$$b = \frac{\alpha}{\beta} = \frac{l_1 I_{12}^2 \sigma_2^2}{l_2 I_{11} I_{22} \sigma_1^2}, \quad (5.6)$$

giving
$$A_3^+ = \frac{4b e^{-il_1 L}}{(1+b)^2 e^{-il_2 L} - (1-b)^2 e^{il_2 L}}, \quad (5.7)$$

$$A_1^- = \frac{-(1-b^2) [e^{-il_2 L} - e^{il_2 L}]}{(1+b)^2 e^{-il_2 L} - (1-b)^2 e^{il_2 L}}. \quad (5.8)$$

The reflection and transmission coefficients are given by

$$K_R^2 = A_1^{-1} A_1^{-*} = \frac{A}{1+A}, \quad K_T^2 = A_3^+ A_3^{+*} = \frac{1}{1+A}, \quad (5.9a, b)$$

where
$$A = \frac{(1-b^2)^2}{4b^2} \sin^2 l_2 L. \quad (5.10)$$

The form of K_R^2 and K_T^2 guarantees conservation of action.

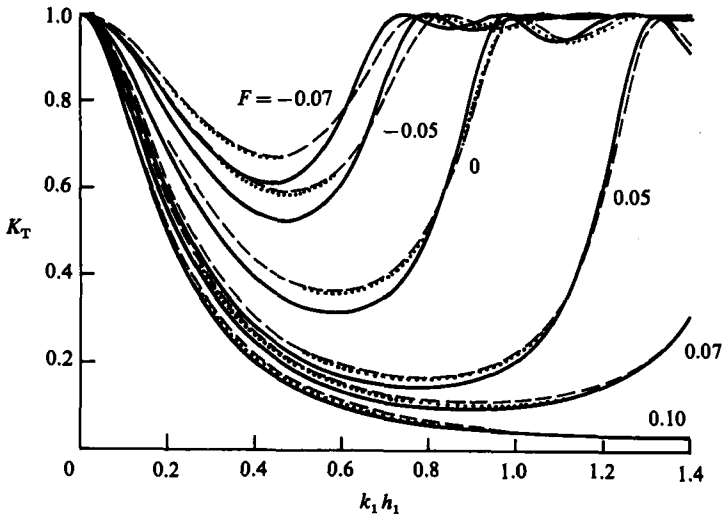


FIGURE 8. Plane-wave approximation for the symmetric trench of figure 6: —, EFEM results; ---, plane-wave approximation (5.4); ·····, action-based model (5.30).

For the case of a single step discontinuity in depth and current, we may set $h_2 = h_3$ and $V_2 = V_3$. The general result (5.4) then reduces to

$$A_3^+ = \frac{2\alpha\beta I_{32}/I_{12}}{\alpha'(\alpha + \beta)}, \quad A_1^- = \frac{\alpha - \beta}{\alpha + \beta}, \quad (5.11)$$

These may be written as

$$A_1^- = \frac{b-1}{b+1}, \quad A_3^+ = \frac{2\gamma b}{b+1}, \quad (5.12)$$

where

$$\gamma = \frac{\beta I_{32}}{\alpha' I_{12}} = \frac{\sigma_1 I_{11}}{\sigma_2 I_{12}}. \quad (5.13)$$

Plots of the plane-wave approximation for a symmetric and asymmetric trench are given in figures 8 and 9 in comparison with the full numerical (EFEM) results. KD1 have already shown that the accuracy of the approximate solution decreases with increasing relative trench depth. The results in figures 8 and 9 indicate also that the approximation is less accurate for opposing currents ($F < 0$) than for following currents ($F > 0$).

The solutions presented above may be developed in the deep-water limit by the revised choice

$$f_{i,0} = e^{k_i z}. \quad (5.14)$$

The resulting integrals taken over the entire water depth are

$$I_{ij} = (k_i + k_j)^{-1}. \quad (5.15)$$

Then we have

$$\left. \begin{aligned} \alpha &= l_1 \sigma_2 \sigma_1^{-1} (k_1 + k_2)^{-2}; & \alpha' &= l_3 \sigma_2 \sigma_3^{-1} (k_2 + k_3)^{-2}, \\ \beta &= l_2 \sigma_1 \sigma_2^{-1} (4k_1 k_2)^{-1}; & \beta' &= l_2 \sigma_3 \sigma_2^{-1} (4k_3 k_2)^{-1}. \end{aligned} \right\} \quad (5.16)$$

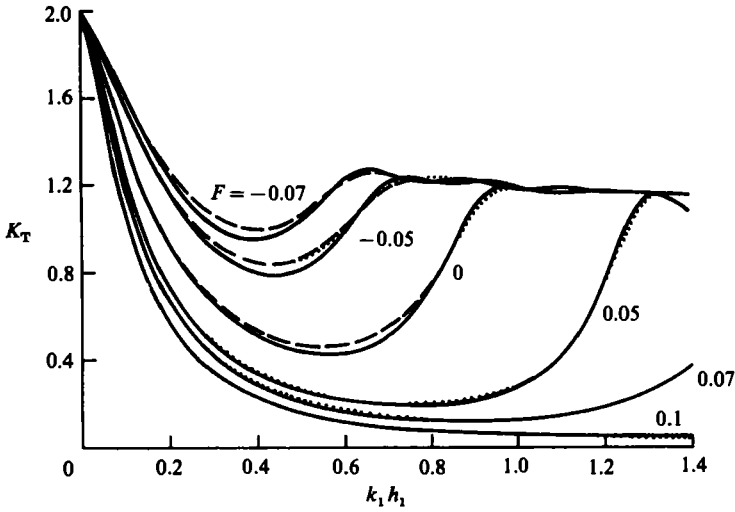


FIGURE 9. Plane-wave approximation for the asymmetric trench of figure 7: —, EFEM results; ---, plane-wave approximation (5.4); ·····, action-based model (5.30).

The plane-wave solution for the case of a single vortex sheet (with properties in regions 2 and 3 taken to be equal) are given by (5.12) with

$$b = \frac{\alpha}{\beta} = \frac{l_1 \sigma_2^2}{l_2 \sigma_1^2} \frac{4k_1 k_2}{(k_1 + k_2)^2}, \quad \gamma = \left(\frac{k_1 + k_2}{2k_1} \right) \frac{\sigma_1}{\sigma_2}. \quad (5.17)$$

The corresponding reflection and transmission coefficients are given by

$$K_R = A_1^- = \frac{b-1}{b+1}, \quad K_T = A_3^+ \left(\frac{\sigma_2}{\sigma_1} \right) = \frac{2b}{b+1} \left(\frac{k_1 + k_2}{2k_1} \right). \quad (5.18)$$

These deep-water results may be compared with the 'action-based' results of Smith (1983). (The general form of the action-based model for the trench will be considered in the following section.) Defining a parameter δ (equal to Smith's α), we get

$$b = \frac{\delta(4k_1 k_2)}{(k_1 + k_2)^2}. \quad (5.19)$$

Smith's results are given by

$$K_R^S = \frac{\delta-1}{\delta+1}, \quad K_T^S = \frac{2\delta}{\delta+1} \left(\frac{k_2}{k_1} \right)^{\frac{1}{2}}. \quad (5.20)$$

A comparison of reflection and transmission coefficients for Smith's model, the present deep-water plane-wave model and Evans' (1975) numerical results is given in figure 10. Each approximate model is a good predictor of transmission coefficient for waves entering a following stream ($V > 0$), and reflection and transmission coefficients for all models are essentially equivalent in the range $|V/C_0| \leq 0.3$, where C_0 is the free-wave speed $(g/k_1)^{\frac{1}{2}}$. (See Smith 1983 for a detailed plot of this region.) Neither approximate model performs well as a predictor of reflection by strong opposing currents, while Smith's model is a better predictor of transmission in this case.

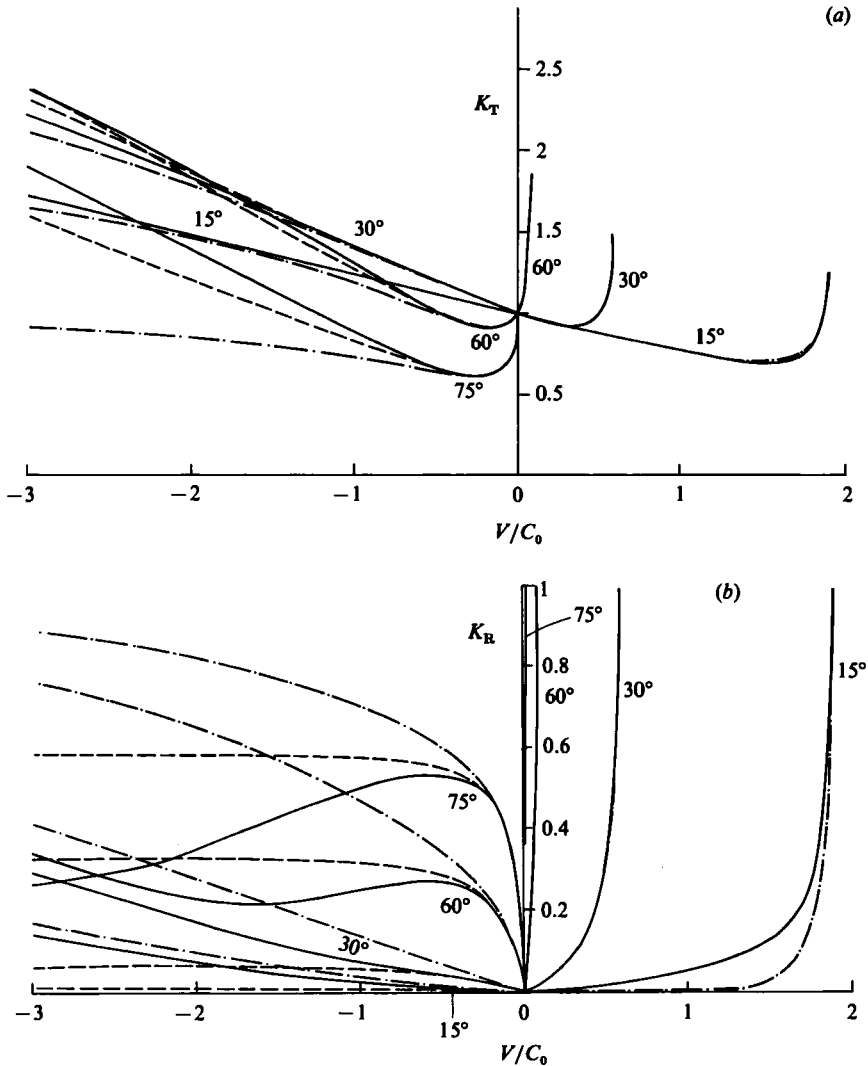


FIGURE 10. Transmission and reflection coefficients for varying angle of incidence θ_1 and normalized current speed V/C_0 : single vortex sheet in deep water. (a) K_T ; (b) K_R . —, Evans (1975); ---, Smith (1983); —·—, present plane-wave approximation.

5.2. Action-based model for a trench

Smith (1987) has extended the 'action-based' model to the case of a single discontinuity in depth and current. We first restate Smith's model for the single step in the present notation and then extend it to the case of the submerged trench.

Referring back to (5.1) and (5.2), we replace the depth averages given there with some unspecified set of averages for the pressure equation, in the form

$$\sigma_1(1 + A_1^-) \langle f_{1,0} \rangle_1 = \sigma_2 A_2^+ \langle f_{2,0} \rangle_1. \quad (5.21)$$

Smith suggests that the average be given by a r.m.s. weighting of each eigenmode over the shallower depth, to give

$$\langle f_{i,0} \rangle_1 = \left\{ \int_{-h_1}^0 f_{i,0}^2 dz \right\}^{\frac{1}{2}}. \quad (5.22)$$

In the present notation, we define

$$\gamma_1 = \frac{\sigma_1 \langle f_{1,0} \rangle_1}{\sigma_2 \langle f_{2,0} \rangle_1} = \frac{\sigma_1 (I_{11})^{\frac{1}{2}}}{\sigma_2 (I_{22})^{\frac{1}{2}}} F_1^{-\frac{1}{2}}, \quad (5.23)$$

where
$$F_1 = \frac{\langle f_{2,0} \rangle_1^2}{I_{22}} = \frac{\sinh 2k_2 h_2 - \sinh 2k_2 (h_2 - h_1) + 2k_2 h_1}{\sinh 2k_2 h_2 + 2k_2 h_2}. \quad (5.24)$$

We write the pressure and velocity matching then as

$$\gamma_1(1 + A_1^-) = A_2^+, \quad \delta_1 \gamma_1(1 - A_1^-) = A_2^+ \quad (5.25 a, b)$$

and obtain

$$A_1^- = \frac{\delta_1 - 1}{\delta_1 + 1}; \quad A_2^+ = \frac{2\delta_1 \gamma_1}{\delta_1 + 1}. \quad (5.26)$$

Using the requirement of action conservation (2.30) then gives

$$\delta_1 = \frac{l_1 \sigma_2^2}{l_2 \sigma_1^2} F_1. \quad (5.27)$$

Turning to the case of a trench with depth h_3 in region 3, we define

$$\gamma_3 = \frac{\sigma_3 (I_{33})^{\frac{1}{2}}}{\sigma_2 (I_{22})^{\frac{1}{2}}} F_3^{-\frac{1}{2}}; \quad F_3 = \frac{\langle f_{2,0} \rangle_3^2}{I_{22}}, \quad (5.28)$$

where the average is now over h_3 at $x = L$. Equations (5.1) and (5.2) are then posed as

$$\gamma_1(1 + A_1^-) = A_2^+ + A_2^-, \quad \gamma_3 A_3^+ e^{i l_3 L} = A_2^+ e^{i l_2 L} + A_2^- e^{-i l_2 L} \quad (5.29 a, b)$$

and

$$\delta_1 \gamma_1(1 - A_1^-) = A_2^+ - A_2^-, \quad \delta_3 \gamma_3 A_3^+ e^{i l_3 L} = A_2^+ e^{i l_2 L} - A_2^- e^{-i l_2 L}. \quad (5.29 c, d)$$

These are solved as in the previous section to obtain

$$A_3^+ = \frac{2\delta_1(\gamma_1/\gamma_3) e^{-i l_2 L}}{(\delta_1 + \delta_3) \cos l_2 L - i(1 + \delta_1 \delta_3) \sin l_2 L} \quad (5.30 a)$$

and

$$A_1^- = \frac{(\delta_3 - \delta_1) \cos l_2 L - i(1 - \delta_1 \delta_3) \sin l_2 L}{-(\delta_3 + \delta_1) \cos l_2 L + i(1 + \delta_1 \delta_3) \sin l_2 L}. \quad (5.30 b)$$

Forcing conservation of action then gives

$$\delta_3 = \frac{l_3 \sigma_2^2}{l_2 \sigma_3^2} F_3 \quad (5.31)$$

and the same expression for δ_1 as given above.

For the case of a symmetric trench, we may take

$$\delta_1 = \delta_3 = \delta, \quad \gamma_1 = \gamma_3 = \gamma, \quad F_1 = F_3 = F. \quad (5.32)$$

The resulting expressions for A_3^+ and A_1^- are given by (5.7) and (5.8) with δ replacing b defined by (5.6).

Results of the action model are included in figures 8 and 9 in comparison with the EFEM and 'plane-wave' approximations. The deviation between the two approximate solutions is small and generally less than the deviation between approximate and EFEM solutions, except in some areas where the three solutions are close. Only the portions of the curves for the action-based results that deviate from curves for the other models by more than the graphical resolution of the figures are plotted.

A similar close correspondence between the plane-wave and action approximations is pointed out in one case by Smith (1987). The action-based approximation generally improves slightly in comparison with the plane-wave approximation as water depth increases. (Recall the deep-water results given above.)

5.3. Variational approximation

Since the action-based model does not provide a significant improvement over the plane-wave approximation for the intermediate-depth case studied above, we have further constructed a variational approximation following the original formulation of Miles (1967). Mei & Black (1969) have extended Miles' (1967) approach to the case of a symmetric obstacle, and Miles (1982) has followed their approach to study the scattering of obliquely incident waves by a symmetric trench (limited to case 1, freely propagating modes in the entire domain). On the other hand, Lassiter (1972) has considered the case of normal incidence on an asymmetric trench. Here, we generalize Miles' method to cover oblique incidence (with l_2 and l_3 possibly imaginary), asymmetric geometry and the presence of currents.

We proceed by specifying the horizontal velocity components divided by intrinsic frequency at $x = 0$ and L as $U_1(z)$ and $U_3(z)$ respectively. Using (2.22) and employing orthogonality conditions leads to the equations

$$il_1(A_1^+ - A_1^-)I_{11} = \sigma_1 \int_{-h_1}^0 U_1(z)f_{1,0}(z) dz, \quad (5.33a)$$

$$\lambda_{1,n} B_{1,n}^+ J_{11}(n) = \sigma_1 \int_{-h_1}^0 U_1(z)f_{1,n}(z) dz, \quad (5.33b)$$

$$il_2(A_2^+ - A_2^-)I_{22} = \sigma_2 \int_{-h_1}^0 U_1(z)f_{2,0}(z) dz, \quad (5.33c)$$

$$\lambda_{2,n}(B_{2,n}^+ - B_{2,n}^-)J_{22}(n) = \sigma_2 \int_{-h_1}^0 U_1(z)f_{2,n}(z) dz \quad (5.33d)$$

for the junction at $x = 0$, and similar equations for $x = L$ with subscripts 1 replaced by 3 and including the phase shifts to the $x = L$ position. Here, the additional integrals are

$$J_{ij}(n) = \int_{(h_i, h_j)_{\min}}^0 f_{i,n}(z)f_{j,n}(z) dz. \quad (5.34)$$

The resulting set of equations (5.33d) and its counterpart at $x = L$ may be used to solve for the $B_{2,n}^\pm$; we obtain

$$B_{2,n}^\pm = \frac{\sigma_2}{2\lambda_{2,n} J_{22}(n) \sinh \lambda_{2,n} L} \left\{ \int_{-h_2}^0 U_3 f_{2,n} dz - e^{\mp \lambda_{2,n} L} \int_{-h_1}^0 U_1 f_{2,n} dz \right\}. \quad (5.35)$$

The explicit expressions for $B_{1,n}^+$, $B_{2,n}^\pm$, $B_{3,n}^-$ may be used in the conditions for continuity of pressure (2.13b); we obtain

$$\begin{aligned} & \sigma_1(A_1^+ + A_1^-)f_{1,0}(z) - \sigma_2(A_2^+ + A_2^-)f_{2,0}(z) \\ & = \int_{-h_1}^0 U_1(\xi) G_{12}(z, \xi) d\xi + \int_{-h_2}^0 U_3(\xi) G_{11}(z, \xi) d\xi \quad (5.36a) \end{aligned}$$

for $x = 0$ and

$$\begin{aligned} \sigma_2(A_2^+ e^{i\lambda_2 L} + A_2^- e^{-i\lambda_2 L})f_{2,0}(z) - \sigma_3(A_3^+ e^{i\lambda_3 L} + A_3^- e^{-i\lambda_3 L})f_{3,0}(z) \\ = \int_{-h_1}^0 U_1(\xi) G_{31}(z, \xi) d\xi + \int_{-h_3}^0 U_3(\xi) G_{32}(z, \xi) d\xi \end{aligned} \quad (5.36b)$$

for $x = L$, where

$$G_{11} = \sum_{n=1}^{\infty} \frac{\sigma_2^2 f_{2,n}(z) f_{2,n}(\xi)}{\lambda_{2,n} J_{22}(n) \sinh \lambda_{2,n} L}, \quad (5.37a)$$

$$G_{12} = - \sum_{n=1}^{\infty} \frac{\sigma_2^2 f_{2,n}(z) f_{2,n}(\xi)}{\lambda_{2,n} J_{22}(n) \tanh \lambda_{2,n} L} - \sum_{n=1}^{\infty} \frac{\sigma_1^2 f_{1,n}(z) f_{1,n}(\xi)}{\lambda_{1,n} J_{11}(n)} \quad (5.37b)$$

and where $G_{31} = G_{11}$ and G_{32} is obtained from G_{12} by a change in subscript 1 to 3. We now expand U_1 and U_3 in terms of the linearly independent amplitudes:

$$U_1(\xi) = (A_1^+ + A_1^-)f_{11}(\xi) + (A_2^+ + A_2^-)f_{12}(\xi), \quad (5.38a)$$

$$U_3(\xi) = (A_3^+ e^{i\lambda_3 L} + A_3^- e^{-i\lambda_3 L})f_{33}(\xi) + (A_2^+ e^{i\lambda_2 L} + A_2^- e^{-i\lambda_2 L})f_{32}(\xi) \quad (5.38b)$$

where the f_{ij} are unknown. Substituting (5.38) in (5.36), adding the two parts of (5.36) and collecting the coefficients of each independent pair of amplitudes produces the following integral equations: from $x = 0$,

$$\sigma_i f_{i,0}(z) = (-1)^{i-1} \int_{-h_1}^0 f_{1i}(\xi) G_1(z, \xi) d\xi; \quad i = 1, 2, \quad (5.39a)$$

and from $x = L$,

$$\sigma_i f_{i,0}(z) = (-1)^i \int_{-h_3}^0 f_{3i}(\xi) G_3(z, \xi) d\xi; \quad i = 2, 3, \quad (5.39b)$$

where $G_i = G_{i2} + G_{i1}$. The integral equations define the unknown f_{ij} . We note that the kernels G_i are symmetric in z and ξ . The set of equations (5.39) are then convolved with each of the independent velocity components to obtain

$$S_{ij}^1 = \int_{-h_1}^0 \sigma_i f_{i,0}(z) f_{ij}(z) dz = (-1)^{i-1} \int_{-h_1}^0 \int_{-h_1}^0 f_{1i}(\xi) G_1(z, \xi) f_{ij}(z) d\xi dz, \quad i = 1, 2; \quad j = 1, 2, \quad (5.40a)$$

$$S_{ij}^3 = \int_{-h_3}^0 \sigma_i f_{i,0}(z) f_{3j}(z) dz = (-1)^i \int_{-h_3}^0 \int_{-h_3}^0 f_{3i}(\xi) G_3(z, \xi) f_{3j}(z) d\xi dz, \quad i = 2, 3; \quad j = 2, 3, \quad (5.40b)$$

where S_{ij}^1 and S_{ij}^3 are the scattering-matrix elements for corresponding single-step problems posed at $x = 0$ and L . Note that $S_{ij}^{13} = -S_{ji}^{31}$ for $i \neq j$, due to symmetry of the kernels. The S_{ij} may be written as stationary variational integrals following Miles (1967), giving

$$S_{ij}^1 = \frac{(-1)^{j-1} \sigma_i \sigma_j \int_{-h_1}^0 f_{i,0} f_{1j} dz \int_{-h_1}^0 f_{j,0} f_{1i} dz}{\int_{-h_1}^0 \int_{-h_1}^0 f_{1i}(\xi) G_1(z, \xi) f_{1j}(z) d\xi dz}, \quad i = 1, 2; \quad j = 1, 2, \quad (5.41a)$$

$$S_{ij}^3 = \frac{(-1)^j \sigma_i \sigma_j \int_{-h_3}^0 f_{i,0} f_{3j} dz \int_{-h_3}^0 f_{j,0} f_{3i} dz}{\int_{-h_3}^0 \int_{-h_3}^0 f_{3i}(\xi) G_3(z, \xi) f_{3j}(z) d\xi dz}, \quad i = 2, 3; \quad j = 2, 3. \quad (5.41b)$$

N	F = 0		F = -0.0525		F = 0.0525	
	K _R	K _T	K _R	K _T	K _R	K _T
1	0.940003	0.341166	0.591586	0.806242	0.989332	0.145678
3	0.941636	0.336631	0.590768	0.806842	0.989665	0.143399
5	0.942039	0.335503	0.590515	0.807026	0.989737	0.142900
7	0.942090	0.335360	0.590485	0.807049	0.989747	0.142832
9	0.942122	0.335271	0.590466	0.807063	0.989753	0.142790
15	0.942165	0.335149	0.590438	0.807083	0.989761	0.142734
% E†	0.082	-0.644	2.074	-1.059	0.005	-0.235

TABLE 2. Convergence of the variational approximation with increasing N: $h_2/h = 3$, $L/h_1 = 10$, $k_1 h_1 = 0.68034$

† Percent error in the 15-term variational solution compared with the 50-term EFEM result.

Substituting these results back into (5.33) for the propagating modes gives, finally, the 4×4 matrix equation for A_1^- , A_2^\pm and A_3^+ , where we have set $A_1^+ = 1$ and $A_3^- = 0$ to represent waves incident from $x = -\infty$ left only:

$$\begin{pmatrix} il_1 I_{11} + S_{11}^1 & S_{12}^1 & S_{12}^1 & 0 \\ S_{12}^1 & il_2 I_{22} - S_{22}^1 & -il_2 I_{22} - S_{22}^1 & 0 \\ 0 & S_{22}^2 e^{il_1 L} & S_{22}^2 e^{-il_1 L} & (S_{33}^3 - il_3 I_{33}) e^{il_1 L} \\ 0 & (S_{22}^2 - il_2 I_{22}) e^{il_1 L} & (S_{22}^2 + il_2 I_{22}) e^{-il_1 L} & S_{21}^3 e^{il_1 L} \end{pmatrix} \begin{pmatrix} A_1^- \\ A_2^+ \\ A_2^- \\ A_3^+ \end{pmatrix} = \begin{pmatrix} il_1 I_{11} - S_{11}^1 \\ -S_{12}^1 \\ 0 \\ 0 \end{pmatrix}. \tag{5.42}$$

This matrix may be inverted, after determination of the S_{ij} , to give the unknown propagating wave amplitudes. In order to evaluate the S_{ij} , we choose to represent the velocities at each junction by the eigenfunction for the propagating wave mode on the shallower side, following Miles (1967) (see also Smith 1987). We thus take

$$f_{1i}(z) = C_i^1 f_{1,0}(z), \quad i = 1, 2; \quad f_{3i}(z) = C_i^3 f_{3,0}(z), \quad i = 2, 3. \tag{5.43}$$

These are substituted into (5.41), leading to immediate cancellation of the scale factors C due to the scale invariance of the variational forms. The S_{ij} are then evaluated after choosing the number of non-propagated modes to retain in truncating the infinite sums to a finite number N of terms.

Numerical tests of convergence of the variational approximation for increasing N are given in table 2, for comparison with EFEM results in table 1. For the relatively small depth changes investigated here, convergence of the variational method is quite rapid, with $N = 5$ being sufficient to obtain three-decimal-place convergence. (A similar convergence criterion applied to the EFEM results indicates that up to ≈ 16 modes are required.) Table 2 also gives percent error in the final $N = 15$ results for the variational approximation in comparison with the $N = 50$ EFEM results. As in the previous two approximate solutions, the greatest deviations between the variational and (presumably more exact) EFEM solutions occur in cases of strong opposing ($F < 0$) currents in the trench. However, variational solutions (even for $N = 1$) are significantly closer to EFEM results than either of the propagating-mode approximations for the entire range of parameters studied. Indeed, the EFEM and variational results are graphically indistinguishable for most of the plotted cases in figures 8 and 9 and thus no additional plots are given.

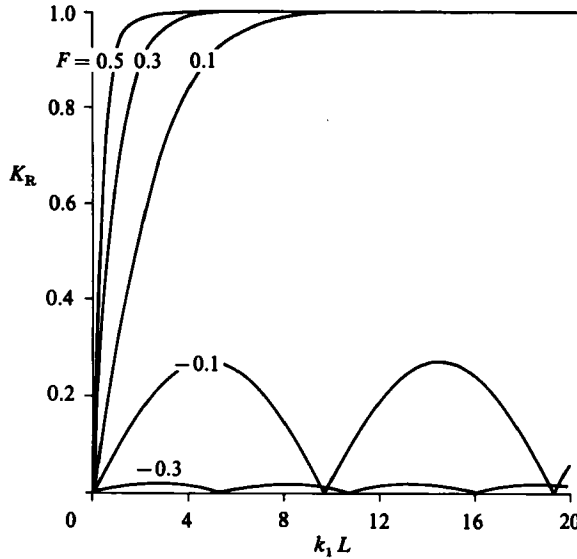


FIGURE 11. Effect of current along the trench on the reflection coefficient K_R in shallow water: $h_2/h_1 = 2$, $\theta_1 = 45^\circ$. Curves for varying $F = V_2/(gh_2)^{1/2}$.

6. Long-wave asymptote

For the case of $kh \ll 1$ in all regions, the plane-wave solution and the 'action-based' model presented above are asymptotic to the same results. The integrals and coefficients in the plane-wave theory reduce to

$$I_{11} = I_{12} = h_1, \quad I_{32} = I_{33} = h_3, \quad I_{22} = h_2 \quad (6.1)$$

and
$$\alpha = \frac{l_1 h_2^2 \sigma_2}{\sigma_1}, \quad \alpha' = \frac{l_3 h_3^2 \sigma_2}{\sigma_3}, \quad \beta = \frac{l_2 h_1 h_2 \sigma_1}{\sigma_2}, \quad \beta' = \frac{l_2 h_2 h_3 \sigma_3}{\sigma_2}. \quad (6.2)$$

For the single vortex sheet with possible change in depth, we obtain the result (5.12) or (5.26) with

$$\delta = b = \frac{l_1 h_1 \sigma_2^2}{l_2 h_2 \sigma_1^2} = \frac{l_1 l_2^2}{l_2 k_1^2}, \quad \gamma = \frac{\sigma_1}{\sigma_2}. \quad (6.3)$$

The results are equivalent to the results in Kirby (1986, equations (3.12) and (3.13)), where solutions were obtained by matching volume fluxes following the wave-distorted vortex sheet, based on Lamb's (1945) hypothesis. The results for a symmetric trench also follow directly from (5.7) and (5.10) with b given by (6.3). Mei & Lo (1984, see corrections 1986) have presented results for a current jet alone ($h_1 = h_2 = h_3$). Several plots of results for varying geometry are given in figures 11–13. Figure 11 indicates the effect of varying current speed on reflection for a fixed boundary geometry, and shows the tendency for opposing currents to reduce reflection by causing Case 1 behaviour in the trench, while for the incident-wave direction and trench configuration considered, following currents all lead to Case 3 behaviour in the trench. Figure 12 shows the effect of increasing trench depth while holding current speed fixed, with deeper trenches leading to more reflection. Finally, figure 13 shows the tendency towards increased reflection with increasing angle of incidence, both for following and opposing currents.

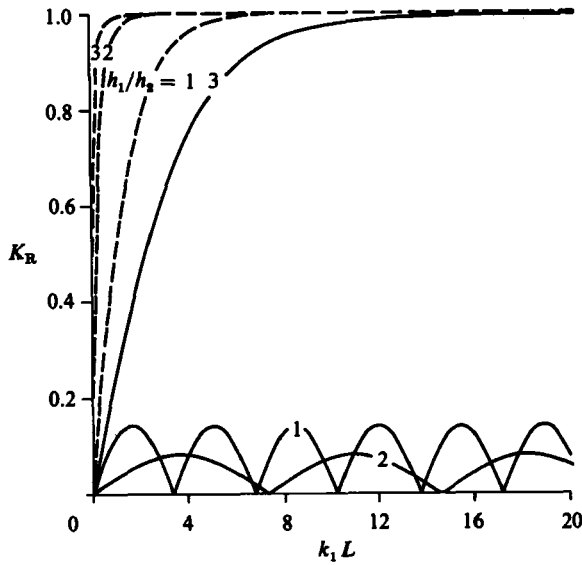


FIGURE 12. Effect of varying trench depth on reflection coefficient K_R in shallow water: $\theta_1 = 60^\circ$. —, opposing current $F = -0.3$; ---, following current $F = 0.3$.

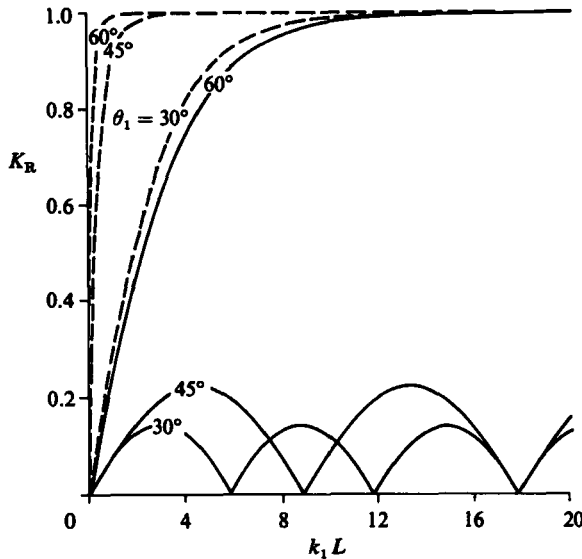


FIGURE 13. Effect of varying angle of incidence on reflection coefficient K_R in shallow water: $h_2/h_1 = 3$. —, opposing current $F = -0.3$; --- following current $F = 0.3$.

7. Conclusions

A method has been developed, based on matched eigenfunction expansions, to study the diffraction of waves by a combination of vortex sheets and depth discontinuities in finite water depth. The eigenfunction method (EFEM) has been verified using a boundary-integral-equation method (BIEM).

Approximate solutions based on truncation of the EFEM solution to its plane-wave

components, and on an application of Smith's (1983) depth-averaging procedure, have been developed and are seen to differ only slightly from each other, while deviations between either propagating-mode approximation and the EFEM solution may be significant over the range of parameters studied. On the other hand, a variational approximation following Miles (1967) is seen to converge quite rapidly and gives results in reasonable agreement with the EFEM method. In terms of computational efficiency and relative accuracy of approximate solutions, the variational method is the strongly preferred of the methods investigated here.

The shallow-water limit of the approximate solutions are investigated and are shown to correspond with the previous results of Kirby (1986).

The numerical results plotted here indicate that the behaviour of waves in the vicinity of submerged trenches or channels in coastal water is likely to be extremely sensitive to even fairly minor variations in flow regime (specifically, to the variation in tidal discharge velocity). It thus seems evident that any modelling effort designed to evaluate wave action in navigation channels, or the effect of such channels on neighbouring regions, should include the possible influence of even small mean water motions in the channel due to tidal activity or steady discharge flows.

REFERENCES

- ABRAMOWITZ, M. & STEGUN, I. A. 1965 *Handbook of Mathematical Functions*. Dover.
- EVANS, D. V. 1975 The transmission of deep-water waves across a vortex sheet. *J. Fluid Mech.* **68**, 389–401.
- KIRBY, J. T. 1986 Comments on 'The effects of a jet-like current on gravity waves in shallow water' *J. Phys. Oceanogr.* **16**, 395–397.
- KIRBY, J. T. & DALRYMPLE, R. A. 1983 Propagation of obliquely incident water waves over a trench. *J. Fluid Mech.* **133**, 47–63.
- LAMB, H. 1945 *Hydrodynamics*, p. 738. Dover.
- LISSITER, J. B. 1972 The propagation of water waves over sediment pockets. Ph.D. dissertation, M.I.T.
- LIU, P. L.-F. & ABBASPOUR, M. 1982 An integral equation method for the diffraction of oblique waves by an infinite cylinder. *Intl J. Num. Meth. Engng* **18**, 1497–1504.
- MEI, C. C. & BLACK, J. L. 1969 Scattering of surface waves by rectangular obstacles in waters of finite depth. *J. Fluid Mech.* **38**, 499–511.
- MEI, C. C. & LO, E. 1984 The effects of a jet-like current on gravity waves in shallow water. *J. Phys. Oceanogr.* **14**, 471–477, and reply to comments, **16**, 1986, 398–399.
- MILES, J. W. 1957 On the reflection of sound at an interface of relative motion. *J. Acoust. Soc. Am.* **29**, 226–228.
- MILES, J. W. 1958 On the disturbed motion of a plane vortex sheet. *J. Fluid Mech.* **4**, 538–552.
- MILES, J. W. 1967 Surface-wave scattering matrix for a shelf. *J. Fluid Mech.* **28**, 755–767.
- MILES, J. W. 1982 On surface-wave diffraction by a trench, *J. Fluid Mech.* **115**, 315–325.
- MOLLO-CHRISTENSEN, E. 1978 Over-reflection of horizontally propagating gravity waves by a vertical shear layer. *Phys. Fluids* **21**, 1908–1911.
- SMITH, J. 1983 On surface gravity waves crossing weak current jets. *J. Fluid Mech.* **134**, 277–299.
- SMITH, J. 1987 On surface waves crossing a step with horizontal shear. *J. Fluid Mech.* **175**, 395–412.
- TAKANO, K. 1960 Effets d'un obstacle parallelepipedique sur la propagation de la houle. *Houille Blanche* **15**, 247–267.
- YEUNG, R. W. 1975 A hybrid integral-equation method for time-harmonic free-surface flow. In *Proc. 1st. Intl Conf. on Num. Ship Hydrodynamics*, pp. 581–607.